Application of a One-Dimensional Dilution and Evaporation Lubricant Oil Model to Predict Oil Evaporation under Different Engine Operative Conditions Considering a Large Hydrogen-Fuelled Engine

2023-24-0009

Application of a one-dimensional dilution and evaporation lubricant oil model to predict oil evaporation under different engine operative conditions considering a large hydrogen-fuelled engine.

Edoardo De Renzis[1], Valerio Mariani[1], Gian Marco Bianchi[1], Stefania Falfari[1], Giulio Cazzoli[1]
[1] Department of Industrial Engineering (DIN), University of Bologna, Alma Mater Studiorum, Italy

Abstract

The increasing environmental concern is leading to the need for innovation in the field of internal combustion engines, in order to reduce the carbon footprint. In this context, hydrogen is a possible mid-term solution to be used both in conventional-like internal combustion engines and in fuel cells (for hybridization purposes), thus, hydrogen combustion characteristics must be considered. In particular, the flame of a hydrogen combustion is less subjected to the quenching effect caused by the engine walls in the combustion chamber. Thus, the significant heating up of the thin lubricant layer upon the cylinder liner may lead to its evaporation, possibly and negatively affecting the combustion process, soot production. The authors propose an analysis which aims to address the behavior of different typical engine oils, (SAE0W30, SAE5W30, SAE5W40) under engine thermo-physical conditions considering a large hydrogen-fuelled engine. The operative conditions are obtained by means of simulations through a zero-dimensional engine model in *OpenWAM* environment. The lubricant oils composition and properties are defined by means of a statistical interference-based optimization approach which identifies the most proper mixture of heavy hydrocarbons as a surrogate of real oils. Then, the mixture is implemented in an in-house developed heat and mass transfer one-dimensional model which accounts for the lubricant oil evaporation and the mutual diffusion between the oil surrogate components. This work aims to test and analyze the response of different lubricant oils to heating and evaporation processes during the compression and combustion stroke of a hydrogen-fuelled internal combustion engine. The behaviour and the properties evolution during the compression and part of the expansion strokes of different lubricant oils in two different engine operative conditions are captured and discussed.

Introduction

In the last decades, the rising public awareness about the impact of the transport sector on the environment has led to the development of new technologies which could satisfy the users power request while keeping pollutant and greenhouse gases emissions as low as possible. These new technologies involve innovative combustion systems, such as Gasoline Compression Ignition (GCI) [1] and Spark-Assisted Compression Ignition (SACI) [2], new thermal management (i.e. High Pressure Direct Injection [3], Water Injection [4], Exhaust Gas Recirculation [5], application of Miller cycle [6] etc.) and control strategies but also the renewal of the traditional carbon fossil fuels paradigm. In this context, hydrogen-fuelled engines are a possible mid-term solution to reduce the transport sector carbon footprint both as stand-alone propulsion devices and in a hybridization strategy with fuel cells. Lubricant oil plays a fundamental role in each of these technologies because of its cooling, lubricating and protection capabilities of the engine mechanical components. Thus, it is crucial to study the behaviour of the lubricant oil and of its properties, for instance viscosity and density, through the life of a propulsion system.

The interaction between traditional fuels, such as gasoline and diesel, and lubricant oil has been studied by many researchers in the past decades due to the effects of this interaction. The generation of the wall film depends on different factors, for instance on the engine and injection system configuration (wall, spray, or air guided) [7]. The fuel impacting the cylinder liner, which is wet by the lubricant oil, dilutes and thickens the lubricant oil layer, thus causing the contamination and thickening of the lubricant layer, causing its degradation and enhancing parts wear [8] [9]. Also, the piston possibly scrapes the accumulated liquid which may be scattered into the piston top land crevice [10] [11]. The lubricant oil/fuel droplets dispersed in the combustion chamber possibly burn according to diffusive flames generating Particulate Matter (PM) [12] or autoignite due to the higher chemical reactivity of the engine oil with respect to the fuel. The droplets autoignition leads to a highly destructive phenomenon known as Low-Speed Pre-Ignition (LSPI), which damages the engine components.

Concerning hydrogen internal combustion engines, the lubricant oil keeps playing its fundamental roles and the interaction with the hydrogen combustion needs to be extensively investigated. At first, it is useful to remember that hydrogen flame is subjected to a smaller quenching distance from the cylinder walls with respect to traditional fossil fuels, thus leading to the heat-up of the lubricant oil layer, affecting its properties and possibly leading to its evaporation.

Hydrogen fuel does not contain carbon atoms, thus molecules containing carbon such as carbon oxide (CO), carbon dioxide (CO2), PM and unburned hydrocarbons (UHC) which are detected at the engine exhaust are assumed to derive from combustion or partial combustion of lubricant oil [13]. It must be considered that hydrogen combustion produces water: due to the short hydrogen flame quenching distance water vapor may interferes with the lubricant oil on the cylinder liner in a cold start or low load operative engine conditions [14]. Also, oil-water emulsion can be caused by the adoption of Direct Water Injection (DWI) in a hydrogen-fuelled engine, with the water being directly injected in the combustion chamber. The typical high temperatures and lean operative conditions of hydrogen combustion tend to enhance the NOx production, which is one of the main drawbacks of this technology. In this context, water injection could be adopted to reduce in-chamber temperature, reducing NOx formation [15] [16]. Oil-water emulsion causes the degradation of some lubricant oil key properties, such as viscosity, possibly enhancing parts wear and friction. In light of above, de-emulsified should be added to lubricant oil for hydrogen combustion

purposes in order to control water ingress [17]. Garcìa et al. [18] studied the lubricant oil pollution in a dual fuel diesel-hydrogen engine. The authors found that metallic components deposited into the lubricant likely due to the hydrogen-oil interaction.

In general, literature provides evidence that further studies on the behaviour of the lubricant oil and its interaction with hydrogen in a hydrogen-fuelled combustion engine are mandatory once engine reliability, emissions and thermal management are considered. Within this frame of reference and considering the experimental difficulties related to investigate such phenomena, a numerical approach based on simulations could be of interest to support new hydrogen propulsion systems and to properly design and choose lubricating oil. Distaso et al. [19] performed zero-dimensional numerical simulations to study the variation of ignition delay time in a hydrogen combustion due to the presence of different amounts of lubricant oil, which influence the charge reactivity. They used a lubricant oil surrogate based on n-hexadecane and developed a reduced reaction mechanism that allowed to discover that lubricant oil significantly facilitates the mixture ignition at lower temperatures with respect to those typical of hydrogen autoignition. Concerning lubricant oil - fuel dilution and fuel evaporation, Mariani et al. [20] [21] developed a one-dimensional lubricant oil – fuel dilution model which is able to qualitatively predict the lubricant oil deterioration due to fuel impact on the cylinder liner wall. Though, attention must be paid on the fact that these models does not account for lubricant oil evaporation, being the characteristic temperatures of gasoline combustion lower with respect to hydrogen combustion, thus not enabling oil evaporation.

In this work, the authors pose further attention to the lubricant oil evaporation and its correlation with a hydrogen-fuelled engine operative conditions, in particular engine load. In order to properly model the thermal behavior of the lubricant oil in such conditions, a preliminary literature review is performed to determine the lubricant oil composition in terms of number and nature of components. Unused lubricant oils are mixtures of several HCs from C14-C16 to C40-C50, plus additives [22] [23]. Then, a set of chosen pure molecules is used to build a lubricant oil surrogate which is able to match a set of the real fluid target properties. The surrogate is achieved through a machine learning-based algorithm which relies on the Bayesian statistical interference for the optimization of oil surrogate mixture composition. This methodology is based on a previous work of the present authors [24]. After a sensitivity test, the number of saturated HCs is determined to limit the size of the set (8 components were chosen). Concerning the choice of the target lubricant oil properties, viscosity, density, thermal conductivity and flash point were selected. These properties were chosen according to literature lubricant oil data availability: in particular, lubricant datasheets usually report two different lubricant oil viscosity, i.e. at 313 K and 373 K, the density at 288 K and the flash point. Further simulation-oriented considerations will be discussed later in this work. This methodology is adopted to achieve the surrogates for three different SAE multigrade lubricant oils, namely a 0W30, a 5W30 and a 5W40 which represent respectively a low, medium and high viscosity and density oils. These three oils are then used in a modified version of the oil-fuel interaction model proposed by the present authors to address lubricant oil evaporation in two different operative conditions in a hydrogen-fuelled ICE.

Methodology

Hydrogen-fuelled engines, due to the hydrogen combustion characteristics, are likely to be affected by lubricant oil evaporation and properties derating. At first, an analysis is performed to define a set of key properties which are involved in the heat and mass transfer and evaporation phenomena. Though, few lubricant oil properties are easily available in literature. For this reason, various lubricant oil manufacturer datasheets were investigated [25], and a properties set was chosen accordingly. Then, a literature review is performed to define the lubricant oil components and to build the optimization database. Once the lubricant oil compositions are determined, the results are used in a one-dimensional mass and heat transfer model, which accounts for oil evaporation, to analyse different lubricant oils behaviour in two engine operative conditions representing a low and a high load engine point. The engine operative conditions are achieved by means of a tuned *OpenWAM* model which provides in-cylinder temperature and pressure to be used, as boundary conditions, in the dilution and evaporation model.

Pure components and properties choices

A literature review has been conducted to define the size of the database and the pure components to consider to model properly the lubricant oil behaviour. As previously mentioned, unused lubricant oil is mainly composed by unbranched hydrocarbons [26]. Concerning unbranched hydrocarbons, normal paraffines from C15 to C45 are found in lubricant oils [22] [26]. Thus, a database composed by normal paraffines ranging from C5 to C45 is considered by the authors.

The choice of the set of lubricant oil properties to be optimized has been made upon practical and thermodynamic considerations. A review of the lubricant oil manufacturer datasheets is performed to understand which properties are usually provided. In this context, a single value of density, two different values for viscosity (i.e. one at 313 K and one at 373 K) and the flash point are selected. Other properties, such as thermal conductivity and normal boiling temperature which are helpful to describe the thermodynamic behaviour of the lubricant oil inside an ICE cylinder, are calculated once the oil composition is defined. Engine oil is responsible for fulfilling two main needs, i.e. lubricating the moving parts thus reducing friction and energy losses, and dissipating part of the heat generated by the combustion. With these regards, it is mandatory to ensure that lubricant oils density and viscosity keep in a confidence operating range. For instance, high-density oil is subjected to lower evaporation rates with respect to a low-density oil. On the other hand, a low-density oil is more able to penetrate engine areas which are difficult to reach. Also, viscosity influences the oil capabilities to adhere to the engine walls and to compensate for the clearance deterioration due to engine aging and to flow through the engine parts. The flash point of a lubricant oil is a fundamental property to help understanding whether a mixture of oil vapor and air is capable of igniting, under the in-cylinder pressure and temperature conditions. In light of the above, viscosity (μ, Eq. (1) from Perry's Handbook [27]), density (ρ, Eq. (2) from [28] and flash point ($T_{F,mix}$, Eq. (3) from [29]) are modelled by means of the following equations respectively.

$$\log \mu = B\left(\frac{1}{T} - \frac{1}{T_O}\right); \quad (1)$$

$$\rho = -3.469 + 0.0006896\,A + \frac{B}{M_w + P} + .. \quad (2)$$
$$+(M_w + P)\,C + D + E;$$

$$T_{F,mix} = \frac{2414}{6.1188 + \log_{10}(I_{mix})} - 230.56; \quad (3)$$

In Eq. (1), viscosity is expressed in cP, T is the temperature in K. T_O and B are constants which accounts for the viscosity dependency on the hydrocarbon carbon number. Density (Eq. (2)) is expressed in g/cm^3, P is the pressure of the system expressed in MPa, M_w is the molecular weight of the normal alkane expressed in g/mol. A, B, C, D, E depend on pressure and temperature. Finally, flash point is expressed in K, being I_{mix} the index for the hydrocarbons' mixture which is known once the volume fractions and the flash point of the components are known.

In this work, three different lubricant oils are considered to address their different behaviour under two different engine operative conditions. Since lubricant oils properties depend on the lubricant oils' composition, which is constituted by a large variety of hydrocarbon molecules and additives not easily accessible, the authors decided to focus on some key and easy to access properties, which are available at a manufacturer website [25] where datasheets are stored. The chosen properties are summarized in Table 1.

Table 1. Selected target properties for the three different lubricant oil surrogates to be optimized.

Properties	**0W30**	**5W30**	**5W40**
Density ($kg\ m^{-3}$) @ 288 K	838.0	841.0	840.0
Viscosity (cP) @ 313 K	47.8	53.7	63.0
Viscosity (cP) @ 373 K	9.2	10.0	11.1
Flash point temp. (K)	499.0	509.0	515.0

Oil surrogate optimization

The optimization of the lubricant oil surrogate is performed with a Bayesian statistical interference methodology. This choice was mainly made because of the highly non-linear relation between oil properties and oil composition together with the size of the domain, i.e. the number of pure molecules available to made the oil surrogate. The algorithm used for the surrogates optimization can be described by four main points: i) initially, a defined number of randomly generated composition sets on which the objective function is evaluated; ii) priors are fit to these random sets according to a Gaussian Process (GP); iii) the sets are used to evaluate the Acquisition Function (AF) (which is a surrogate function tested in place of the optimization function if the latter is complex with unknown behavior over the domain); iv) the latest evaluated set of points allows to update the priors to posteriors, then, the workflow is repeated based on those new points. In this framework, GP were a suitable option since they precisely interpolate the new observations while providing both new values and their confidence interval, being probabilistic algorithms. As acquisition function, the upper confidence bound was chosen. This function ($\mu(x) + \theta \cdot K(x)$) uses the mean ($\mu$) and the covariance ($K$) of the GP and a parameter for tuning the split between exploitation and exploration phases (θ). The higher is the θ-value, the more the algorithm explores regions of the domain with high uncertainty, in which the optimal composition may fall. For oil surrogate application, a 8-dimension domain has been chosen given by the following selection of saturated hydrocarbons: pentane (C_5H_{12}); pentadecane ($C_{15}H_{32}$); eicosane ($C_{20}H_{42}$); pentacosane ($C_{25}H_{52}$); triacontane ($C_{30}H_{62}$); pentatriacontane ($C_{35}H_{72}$); tetracontane ($C_{40}H_{82}$); pentatetracontane ($C_{45}H_{92}$). In this work, the number of initial random sets is 50, the θ-value is 0.5, regarding the stop criterion, the algorithm evaluates new points up to 250 epochs.

The objective function to be maximized is reported in equation 4: e is the relative error for each target property expressed as [reference value – calculated value]/reference value x 100, W is the respective weight, tuned by the authors in line with the analysis of intermediate results in order to give more emphasis to the targets that are harder to capture. The targets chosen to mimic the oil behavior are the liquid phase density (ρ), the dynamic viscosity (μ) at low load-like temperature and high load-like temperature, the flash point (Flash Point Temperature, FPT). The final set of weights (W, in Eq. (4)) associated to the abovementioned target properties is 1.1, 1.2, 1.1, 1.0, respectively. According to Eq. (4), the objective function is an Euclidean distance which will be minimal for the optimum mixture. Thus, the optimum surrogate is the composition which maximizes the value of the F function. Due to the statistical base of the methodology, repeated runs of the optimizer with fixed parameters, results in different optimum surrogate identification. The convergence of the set is achieved when the surrogates associated to the higher scores of F have similar compositions.

$$F = 100 - \left(\frac{\sqrt{W_1 \cdot e_\rho^2}}{\sqrt{\sum_i W_i}} + \frac{\sqrt{W_2 \cdot e_{\mu@313}^2}}{\sqrt{\sum_i W_i}} + .. \right.$$
$$\left. + \frac{\sqrt{W_3 \cdot e_{\mu@373}^2}}{\sqrt{\sum_i W_i}} + \frac{\sqrt{W_3 \cdot e_{FPT}^2}}{\sqrt{\sum_i W_i}}\right) \quad (4)$$

Diffusion and evaporation model

The methodology discussed above focuses on the achievement of the lubricant oil compositions upon the choice of a thermodynamic properties set. These compositions are needed as inputs in a mass and thermal diffusion and evaporation numerical model, now briefly described. This model relies on a previous work by the present authors [20] and allows to evaluate the lubricant oil evaporation, while accounting for the mutual diffusion among its components and the temperature dependency of its properties during the working cycle of a hydrogen-fuelled ICE. The computational domain is composed by the cylinder liner wall, the lubricant oil layer and a moving boundary to address lubricant oil evaporation, thus, the layer thickness reduction during the simulation. The discretization of the

domain is one-dimensional along the radial dimension. Figure 1 shows domain, where SLI and LGI are the Solid-Liquid Interface and the Liquid-Gas Interface.

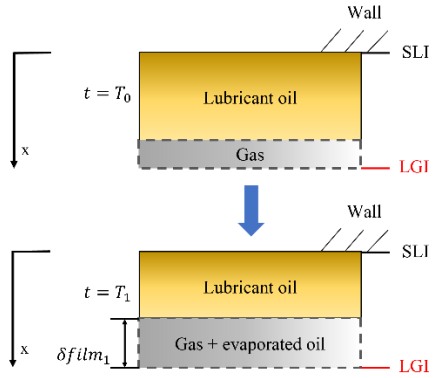

Figure 1. Schematic representation of the computational domain, from the cylinder liner wall to the gas and of the lubricant oil evaporation mechanism. The SLI is the Solid-Liquid Interface and the LGI is the Liquid-Gas Interface.

The main assumptions for the present model are the following: a) the phenomena of interest (oil components mutual diffusion, oil evaporation) occurs only along the radial direction, thus, considerations are made on the oil layer per unit area; b) the oil layer is considered as a thin film; c) no viscous dissipation; d) the heat exchange between solid (cylinder liner) and liquid (oil layer) is due to conduction only, thus, no liquid motion is considered; e) the coolant-side solid layer is considered at fixed temperature equal to that of the coolant; f) oil consumption is due to evaporation only; g) gas and vapours are considered as perfect gases.

The heat transfer is modelled as pure conductive both through the solid layer, through the liquid layer and at the SLI according to the Fourier's equation (Eq. (5)). In Eq. (5), T is the temperature, α is the thermal diffusion coefficient. The mass transfer by diffusion in the liquid phase is modelled with the second Fick's law (Eq. (6)), in which D is the binary diffusion coefficient estimated according to the correlation by Siddiqi and Lucas [30] (chosen in the light of the considerations made in [31]) and ξ is the mass concentration of each component. Furthermore, the mass transfer due to oil liquid-vapor phase change is considered at the LGI by means of Eq. (7), in which T_G is the gas temperature from the engine simulation and H is the convective heat transfer coefficient from the Woschni's correlation [32]. The evaporation of a component of the oil surrogate occurs if the liquid film temperature in the last element of the grid is higher than that of the saturation temperature of the component calculated at the instantaneous cylinder pressure. For numerical stability reasons, the evaporating cell is actually removed when an imposed cell thickness threshold is reached. The threshold is set at the 30 % of the initial cell thickness, i.e. 0.03 µm. It may happen that the cell shrinking exceeds the threshold without exceeding the cell size. In this case, the liquid cell is removed, and the remaining liquid mass is merged in the adjacent cell and the mass concentration is adjusted.

$$\frac{dT}{dt} = \alpha \frac{d^2T}{dx^2} \tag{5}$$

$$\frac{d\xi_i}{dt} = D \frac{d^2\xi_i}{dx^2} \tag{6}$$

$$k \frac{dT}{dx} = H(T - T_G) \tag{7}$$

The simulation time covers the span of the compression stroke and the very first part of the expansion stroke. It is assumed to observe the behavior of the oil layer element at the top dead center. The fate of oil elements of the film layer covered by the piston stroke can be obtained simply considering a shorter simulation time equal to the time at which the piston reaches a specific axial coordinate. An initial oil thickness of 4 µm according to [33] [34] [35]. In order to capture diffusion phenomena related to the oil components, the grid size has been set to 0.1 µm. The simulation time step has been chosen after computational and optimization considerations based on the Courant-Friederichs-Lewy stability condition in thermal problems [36] resulting in a fixed time step of 0.1 µs.

Engine characteristics and operative conditions

The diffusion and evaporation one-dimensional model needs in-cylinder pressure and temperature as boundary conditions in the whole simulation range. An *OpenWAM* [37] model, shown in Figure 2, is used to accomplish this goal. The *OpenWAM* model has been developed by adjusting and modifying an existing four-cylinder automotive engine model. The engine geometry and the operative conditions have been taken from the reference work [38], as well as the double Wiebe configuration and the two Wiebe parameters. Figure 3 shows the comparison between the reference and the *OpenWAM* model calculated in-cylinder pressures adopted for the model validation. The validation was performed following a operative and boundary conditions setup discussed in the reference work [38]. The main characteristics of the hydrogen-fuelled engine are based on the marine lean-burn spark ignition (SI) engine of the work [38] and are summarized in Table 2. A maritime engine has been chosen because its operating windows is quite limited while operating with natural gas. In this context, hydrogen lean burn combustion seems to be an attractive solution [38].

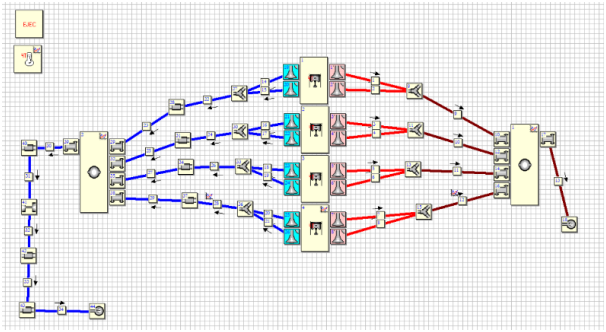

Figure 2. *OpenWAM* model used to obtain the boundary conditions for the dilution/evaporation model.

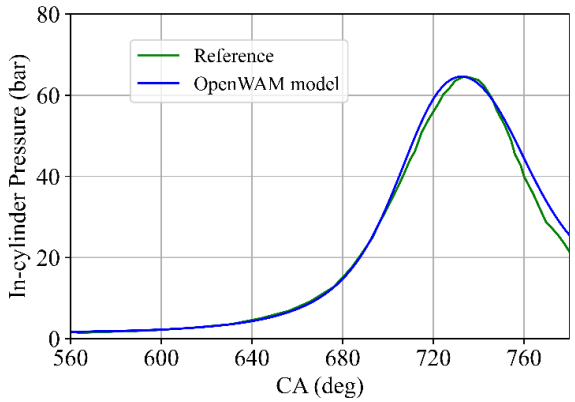

Figure 3. Comparison between the reference and the *OpenWAM* model calculated in-cylinder pressures.

Table 2. Main specification of the hydrogen-fuelled engine used in this work and based on [38].

Parameters	**Specifications**
Displacement	4313 cm^3
Bore x Stroke	170 mm x 190 mm
Geometric Compression Ratio	12:1
Engine speed	1500 rpm
Boost Pressure	1.2 bar, 1.8 bar
Intake air temperature	308 K
Coolant temperature	313 K, 363 K
BMEP	6.7 bar, 18.0 bar
Piston, cylinder temperatures	493 K-393 K, 533 K-413 K
Air-to-fuel ratio	1.6

Two different operative conditions are simulated, which differs from the validation test case: the first one addresses a low load-low speed engine condition with a Break Mean Effective Pressure (BMEP) of 6.7 bar, a boost pressure of 1.2 bar, a coolant, piston and cylinder temperatures of 313 K, 493 K and 393 K; the second one is a high load-low speed engine condition with a BMEP of 18 bar, a boost pressure of 1.8 bar, and a coolant, piston and cylinder temperatures of 363 K, 533 K and 413 K. Also, hydrogen ICE usually works on ultra lean operative conditions, hence an air-to-fuel ratio of 1.6 is assumed. Figure 4 shows the in-cylinder pressures and temperatures for both cases.

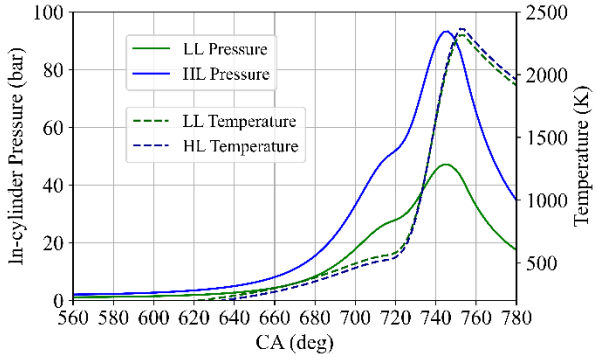

Figure 4. Pressure and temperature for the two simulated hydrogen-fuelled engine operative conditions. LL is low-load, HL is high-load.

Results

In this section the results of the lubricant oil optimization and of the one-dimensional lubricant oil diffusion and evaporation are presented. The methodology described above allows to define the compositions of different lubricant oils once some key target properties are defined through a Bayesian-based optimization. The compositions, along with in-cylinder pressure and temperature achieved by means of a *OpenWAM* model, are used by the diffusion model as initial and boundary conditions. Then, the multicomponent diffusion and evaporation simulations are performed to study the influence of the engine operative conditions, i.e. pressure and temperature, and the lubricant oil composition on its properties in a hydrogen-fuelled engine cycle and to address its evaporation.

Figure 5 shows the percentages errors which are evaluated as ((surrogate – target)/target x 100), where surrogate is the property calculated by means of the optimization process and target is the target property. Also, the objective function is shown.

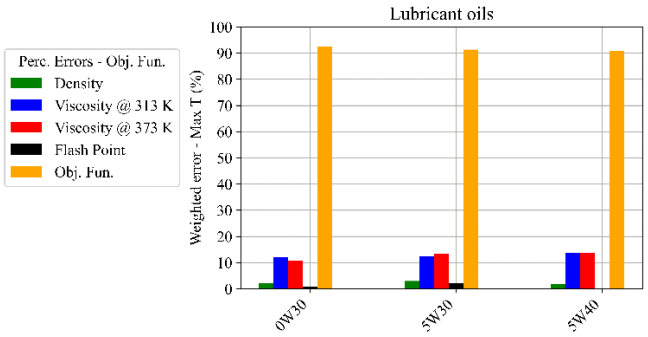

Figure 5. Properties percentages errors and objective functions for the three different lubricant oils.

Figure 6 presents the achieved surrogates' compositions. For each of the three lubricants, the errors on viscosities are slightly above the 10 %, while the errors on density and flash point are much lower. This behaviour is possibly related to the fact that viscosity is strictly related to the presence of lubricant oil additives, which are not modelled in this work. Objective function keeps above the 90 % in every case, thus the achieved surrogates are acceptable. The composition of the 5W30 is the most "balanced", in a components' perspective, because of its properties' characteristics with respect to

the 0W30 and the 5W40. Also, the 5W40 shows the highest percentages of heavier components, due to its higher viscosities.

Concerning the lubricant oil one-dimensional simulation, Figure 7 shows the film temperatures at different distances from the cylinder liner wall and the film thickness evolution during the compression and combustion phases for the SAE 0W30. The film starts noticeably evaporating only after the film reaches a temperature of ≈ 500 K, during the compression stroke. Figure 8, Figure 9 and Figure 10 show the comparisons of the film mean temperatures, viscosities and thicknesses respectively for the optimized and tested lubricant oils, namely a SAE 0W30, a SAE 5W30 and a SAE 5W40.

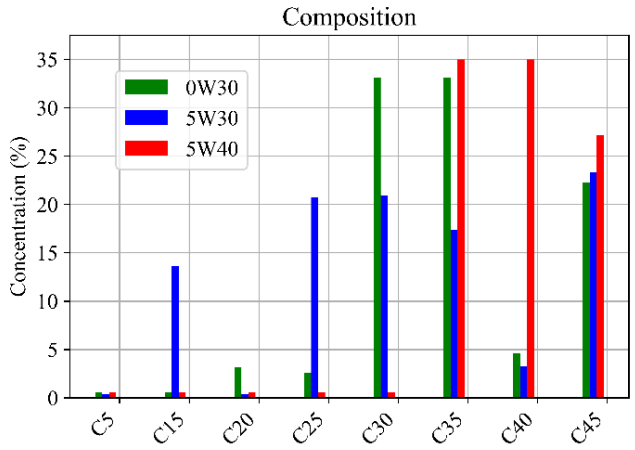

Figure 6. Compositions achieved after the optimization process.

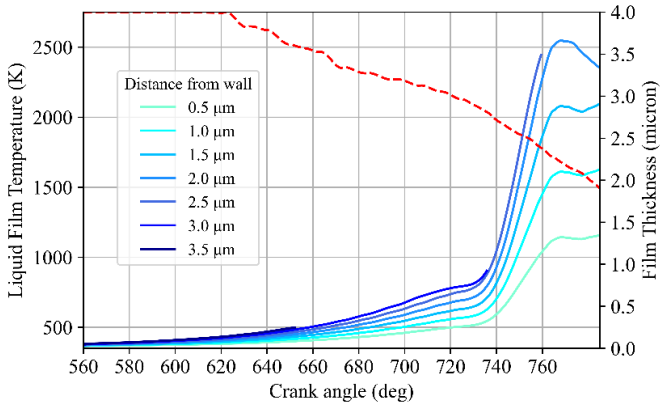

Figure 7. Film temperatures profiles at different distances from the cylinder liner wall and film thickness evolutions during the one-dimensional lubricant oil diffusion and evaporation simulation.

The liquid film mean temperatures (Figure 8) are around 50 K higher in the high engine load operative condition with respect to the low engine operative condition for the tested oils respectively. A slight temperature difference (≈ 5÷10 K) is also observable when different oils are considered: this is due to the different lubricant oils thermal conductivities, which affect the heat transfer.

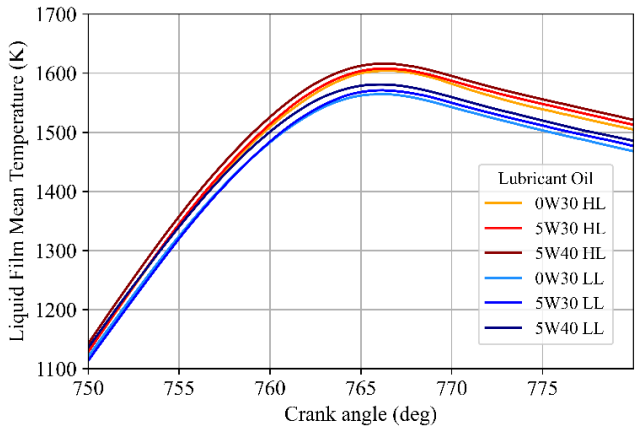

Figure 8. Temperature profiles comparison for the tested lubricant oils.

Figure 9 shows the comparison of the lubricant oil viscosities for the two tested engine operative conditions. The lowest temperatures of the lower engine load lead to initially higher viscosities which decrease drastically during the simulation and due to the rising in-cylinder temperatures. At simulation start, the influence of the lubricant oil composition affects the initial viscosities, while no sensible differences are noticeable among the different cases at the end of the simulation due to the high reached temperatures.

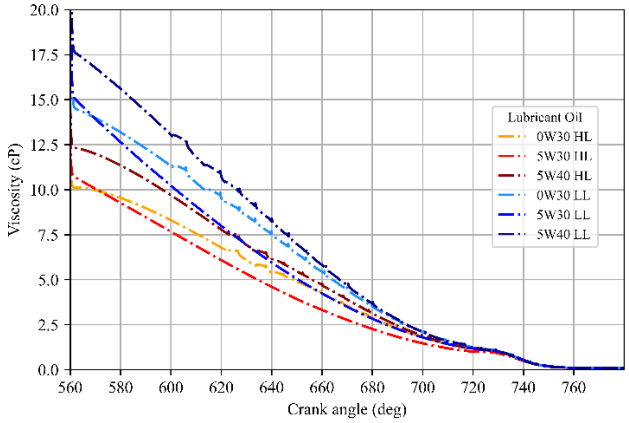

Figure 9. Viscosity profiles comparison for the tested lubricant oils.

Finally, the lubricant oils thicknesses, initially equal to 4 µm, are shown in figure 10. The lubricant oils diffusion and evaporation behaviors are strictly related to their compositions. As previously shown in Figure 5, both lower and higher carbon number hydrocarbons are present in the SAE 5W30, while the SAE 0W30 and the SAE 5W40 are composed mainly of heavier hydrocarbons. Though, being especially the SAE 5W40 subjected to slightly higher temperature due to its higher thermal conductivity, it tends to evaporate more with respect to the SAE 5W30. The higher temperature and pressure of the HL case with respect to the LL case does not show a noticeable difference in terms of film evaporation. This is due to the fact that, especially for the heaviest molecules, the evaporation is subjected to really high temperatures. Hence, the evaporation of these components starts only during the end of the compression stroke and the temperature difference of ≈ 50 K does not have noticeable effects for the limited time until simulation end. Considering for instance the SAE 0W30 case, saturation pressures of the C25, C35 and C45 hydrocarbon molecules are still very low at

720 CAD for both the high load and the low load operative conditions. This means that these components are still non evaporating despite an in-cylinder pressure difference of ≈ 20 bar.

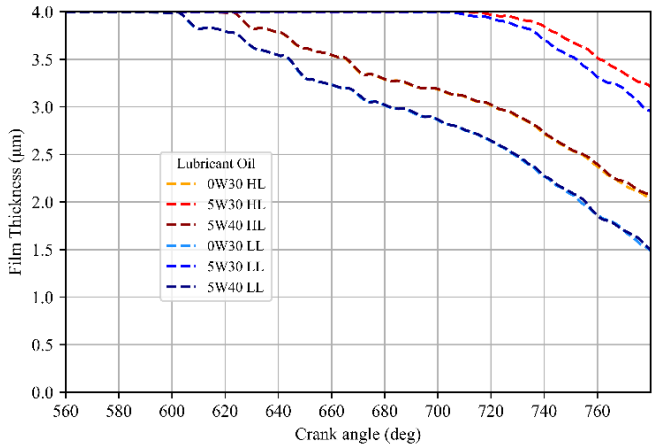

Figure 10. Thicknesses comparison for the tested lubricant oils.

With regards on the multicomponent dilution between the SAE 0W30 lubricant oil components and their evaporation, Figure 11 and Figure 12 provide the evolution of the mass concentration of the lubricant oil components at a distance of 0.05 μm with respect to the liner wall and the evaporation rates of the components during the HL simulation. The lighter molecules show a higher tendency to evaporate, as expected, while the heavier ones are subjected to lower evaporation rates and they start evaporating only when the lubricant layer reaches high temperatures which are typical of the second part of the compression stroke. Also, the evaporation rate of the C5 component shows its maximum during the compression stroke, while it starts to decrease before the top dead center. The evaporation rate is governed by the mass concentration difference of the component between the gas and the liquid phase, hence if this difference becomes lower and lower due to evaporation, the evaporation rate tends to decrease.

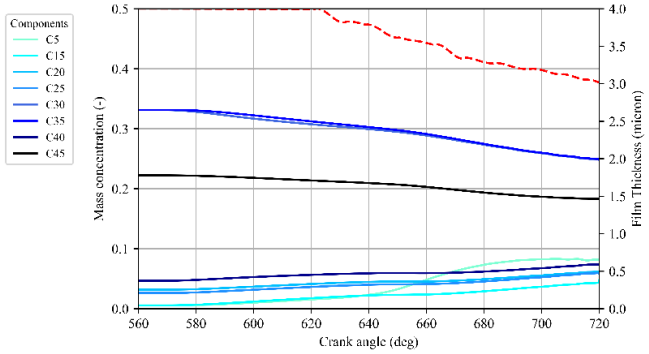

Figure 11. Mass concentration evolution of the SAE 0W30 lubricant oil components at a distance of 0.05 μm with respect to the cylinder liner during the HL simulation.

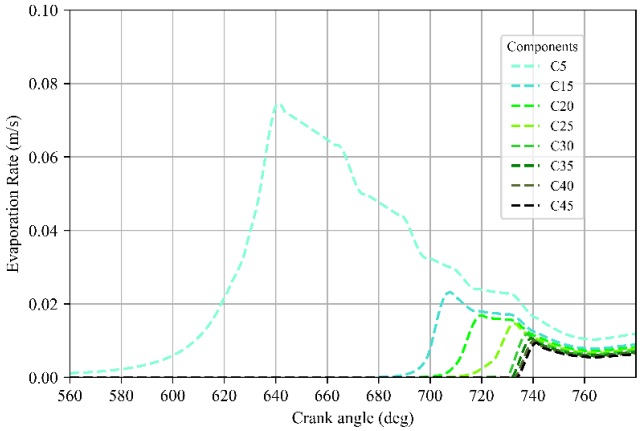

Figure 12. Evaporation rates evolution of the SAE 0W30 lubricant oil components during the HL simulation.

Conclusions

This work focuses on the testing of a numerical methodology which aims i) to optimize the composition and the ii) the numerical description of the thermal behavior of a commercial engine oil assuming an hydrogen-fuelled engine. Surrogates of three different lubricant oils (SAE 0W30, SAE 5W30, SAE 5W40) are provided to a 1D multicomponent oil diffusion and evaporation model. Heat and mass transfer involving the oil film on the cylinder wall are predicted by means of the 1D model.

The simulations results show that the model is able to capture the influence of different lubricant oil composition and engine operative conditions on the lubricant properties and behavior. For instance, the different lubricant oils viscosities are captured, as well as the evaporation rates of the components. The heavier molecules are less likely to evaporate, while the lighter ones start to evaporate before the compression stroke due to the heat transfer from the wall to the liquid film. The pressure and temperature differences between the high-load and the low-load engine conditions did not substantially affect the lubricant oil response, in particular concerning the evaporation. On the other hand, the lubricant oil compositions had a more noticeable impact.

In spite of the fact that a direct validation of the model is not provided due to the lack of experimental data for a fair comparison, the presented methodology can address different tasks in the early development and testing steps of hydrogen engines. As an example, it can be used to determine the likelihood of oil-induced PM formation for a given hydrogen engine configuration. This can be done by using Yield Soot Tendency correlations that usually require information on composition, molecular structure and properties of the hydrocarbons source, which are returned by the methodology thanks to the surrogate definition and dilution-evaporation model. Furthermore, the effect of operating gases with large water content (water would be the only combustion product in H2-engines) can be assessed by implementing the Henry's law at the oil layer moving boundary in order to calculate the water absorption in the multi-component oil. Eventually, in the perspective of evaluating local effects of hydrogen combustion on the oil layer (short quenching distance), the code can be provided with the burned gas temperature profile from CFD engine simulations.

References

1. Rose, K., Ariztegui, J., Cracknell, R., Dubois, T. et al., "Exploring a Gasoline Compression Ignition (GCI) Engine Concept," SAE Technical Paper 2013-01-0911, 2013, https://doi.org/10.4271/2013-01-0911.
2. Robertson, D. and Prucka, R., "A Review of Spark-Assisted Compression Ignition (SACI) Research in the Context of Realizing Production Control Strategies," SAE Technical Paper 2019-24-0027, 2019, https://doi.org/10.4271/2019-24-0027.
3. Spicher, U., Magar, M., and Hadler, J., "High Pressure Gasoline Direct Injection in Spark Ignition Engines - Efficiency Optimization through Detailed Process Analyses," *SAE Int. J. Engines* 9(4):2120-2128, 2016, https://doi.org/10.4271/2016-01-2244.
4. Falfari, S., Bianchi, G., Cazzoli, G., Ricci, M. et al., "Water Injection Applicability to Gasoline Engines: Thermodynamic Analysis," SAE Technical Paper 2019-01-0266, 2019, https://doi.org/10.4271/2019-01-0266.
5. Climent, H., Dolz, V., Pla, B., González-Domínguez, D., "Analysis on the potential of EGR strategy to reduce fuel consumption in hybrid powertrains based on advanced gasoline engines under simulated driving cycle conditions,", Energy Convers. Manage., 266, 2022, doi.org/10.1016/j.enconman.2022.115830.
6. Tavakoli, S., Ali Jazayeri, S., Fathi, M., Jahanian, O., "Miller cycle application to improve lean burn gas engine performance," Energy, 109, 190-200, 2016, https://doi.org/10.1016/j.energy.2016.04.102.
7. Chung, J., Kim, N., Choi, H., and Min, K., "Study on the Effect of Injection Strategies on Particulate Emission Characteristics under Cold Start Using In-cylinder Visualization," SAE Technical Paper 2016-01-0822, 2016, https://doi.org/10.4271/2016-01-0822.
8. Shanta, S. M., Molina, G. J., Soloiu, V., "Tribological Effects of Mineral-Oil Lubricant Contamination with Biofuels: A Pin-on-Disk Tribometry and Wear Study," Adv. Tribology, 1-7, 2011, doi.org/10.1155/2011/820795.
9. Cousseau, T., Juan Sebastian Ruiz, A., Sinatora, A., "Tribological response of fresh and used engine oils: The effect of surface texturing, roughness and fuel type," Tribology Int., 100, 60-69, doi.org/10.1016/j.triboint.2015.11.016.
10. Dahnz, C., Han, K., Spicher, U., Magar, M. et al., "Investigations on Pre-Ignition in Highly Supercharged SI Engines," SAE Int. J. Engines, 3(1):214-224, 2010, https://doi.org/10.4271/2010-01-0355.
11. Amann, M., Alger, T., Westmoreland, B., and Rothmaier, A., "The Effects of Piston Crevices and Injection Strategy on Low-Speed Pre-Ignition in Boosted SI Engines," SAE Int. J. Engines 5(3):1216-1228, 2012, https://doi-org/10.4271/2012-01-1148.
12. Raza, M., Chen, L., Leach, F., Ding, S., "A Review of Particulate Number (PN) Emissions from Gasoline Direct Injection (GDI) Engines and Their Control Techniques," Energies, 11, 1417, 2018, https://doi.org/10.3390/en11061417.
13. Miller, A. L., Stipe, C., Habjan, M. C. and Ahlstrand, G. G., "Role of lubrication oil in particulate emissions from a hydrogen-powered internal combustion engine," Env. Sci. Tech., 41, 19, 6828-6835, 2007, doi:10.1021/es070999r.
14. Singh, S., Bathla, V., Mathai, R., and Subramanian, K., "Development of Dedicated Lubricant for Hydrogen Fuelled Spark Ignition Engine," SAE Technical Paper 2019-28-2511, 2019, https://doi.org/10.4271/2019-28-2511.
15. Younkins, M., Wooldridge, M., and Boyer, B., "Port Injection of Water into a DI Hydrogen Engine," SAE Technical Paper 2015-01-0861, 2015, doi:10.4271/2015-01-0861.
16. Rouleau, L., Duffour, F., Walter, B., Kumar, R. et al., "Experimental and Numerical Investigation on Hydrogen Internal Combustion Engine," SAE Technical Paper 2021-24-0060, 2021, doi:10.4271/2021-24-0060.
17. Singh, S., Bathla, V., Mathai, R., and Subramanian, K., "Development of Dedicated Lubricant for Hydrogen Fuelled Spark Ignition Engine," SAE Technical Paper 2019-28-2511, 2019, doi:10.4271/2019-28-2511.
18. Pardo-García, C., Orjuela-Abril, S., and Pabón-León, J., "Investigation of Emission Characteristics and Lubrication Oil Properties in a Dual Diesel–Hydrogen Internal Combustion Engine," Lubricants, 10(4), 59, doi:10.3390/lubricants10040059.
19. Distaso, E., Calò, G., Amirante, R., De Palma, P. et al. "Highlighting the Role of Lubricant Oil in the Development of Hydrogen Internal Combustion Engines by means of a Kinetic Reaction Model," J. Phys.: Conf. Ser., 2385, 2022, doi:10.1088/1742-6596/2385/1/012078.
20. Mariani, V., Bianchi, G. M., Cazzoli, G. and Falfari, S., "A one-dimensional model for the motor oil-fuel dilution under gasoline engine boundary conditions," E3S Web of Conferences, 197, 2020, doi:10.1051/e3sconf/202019706004.
21. De Renzis, E., Mariani, V., Bianchi, G. M., Falfari and S., Cazzoli, G., "Application of a one-dimensional fuel-oil dilution model coupled with an empirical droplet-to-film formation strategy for predicting in-cylinder oil effects in a direct injection engine," J. Phys.: Conf. Ser., 2385, 2022, doi: 10.1088/1742-6596/2385/1/012063.
22. Wang, F. C. and Zhang, L., "Chemical Composition of Group II Lubricant Oil Studied by High-Resolution Gas Chromatography and Comprehensive Two-Dimensional Gas Chromatography," Energy Fuels, 21, 6, 3477-3483, 2007, doi: 10.1021/ef700407c.
23. Manheim, J., Zhang, Y., Viidanoja, J. et al., "An Automated Method for Chemical Composition Analysis of Lubricant Base Oils by Using Atmospheric Pressure Chemical Ionization Mass Spectrometry," J. Am. Soc. Mass Spectrom., 30, 2019, doi:10.1007/s13361-019-02284-6.
24. Mariani, V., Pulga, L., Bianchi, G. M., Falfari, S., Forte, C., "Machine Learning-Based Identification Strategy of Fuel Surrogates for the CFD Simulation of Stratified Operations in Low Temperature Combustion Modes," Energies, 14(15), 2021, doi: 10.3390/en14154623.
25. https://www.shell.it/motorists/oli-motore-e-lubrificanti-shell.html
26. Lu, S., and Kaplan R. I., "Characterization of Motor Lubricating Oils and Their Oil–Water Partition," Env. Forensics, 9, 295-309, 2008, doi:10.1080/15275920802119441.
27. Green, D. W., "Perry's Chemical Engineers' Handbook," McGraw-Hill, 1997
28. Shahabi-Ghahfarokhy, A., Nakhaei-Kohani, R., Nait Amar, M. and Hemmati-Sarapardeh, A., "Modelling density of pure and binary mixtures of normal alkanes: Comparison of hybrid soft computing techniques, gene expression programming, and equations of state," J. of Petrol. Sci. Eng., 208, 2022, doi: 10.1016/j.petrol.2021.109737.
29. Vidal, M., Rogers, W. J., Holste, J. C. and Mannan, M. S., "A review of estimation methods for flash points and flammability limits," Proc. Safety Prog., 23(1), 47-55, 2004, doi: 10.1002/prs.10004.

30. M. A. Siddiqi et al., Correlations for prediction of diffusion in liquids., Canadian J. of Chem.ical Eng., 64, 839-843, 1986.
31. Mariani, V. et al., Neural Network-Based Prediction of Liquid-Phase Diffusion Coefficient to Model Fuel-Oil Dilution on Engine Cylinder Walls, SAE Int. J. Engines, 3(5), 2020, doi:10.4271/03-13-05-0041
32. Woschni, G., A Universally Applicable Equation for the Instantaneous Heat Transfer Coefficient in the Internal Combustion Engine, SAE Tech. Paper 670931, 1967, doi:10.4271/670931
33. Ilanthirayan, P., et al., Wear Analysis of Top Piston Ring to Reduce Top Ring Reversal Bore Wear, Tribology Industry, 39(4), 487-494, doi:10.24874/ti.2017.39.04.08.
34. Zhang, Q., Kalva, V.T., and Tian, T., "Modeling the Evolution of Fuel and Lubricant Interactions on the Liner in Internal Combustion Engines," SAE Technical Paper 2018-01-0279, 2018, doi:10.4271/2018-01-0279.
35. Vlădescu, S., Medina, S, Olver, A. V., Pegg and, Reddyhoff, T., "Lubricant film thickness and friction force measurements in a laser surface textured reciprocating line contact simulating the piston ring-liner pairing", Tribology Int., 98, 317-329, 2016, doi:10.1016/j.triboint.2016.02.026.
36. Crank, J., Nicolson, P., A practical method for numerical evaluation of solutions of partial differential equations of the heat-conduction type, Adv. Comput. Math., 6, 207-226, 1996, doi:10.1007/BF02127704.
37. www.Openwam.org, OpenWAM, CMT-Motores Térmicos Universitat Politécnica de València (UPV).
38. Sapra,H., Godjevac, M., De Vos, P., Van Sluijs, W., Linden, Y. and Visser, K., "Hydrogen-natural gas combustion in a marine lean-burn SI engine: A comparitive analysis of Seiliger and double Wiebe function-based zero–dimensional modelling," Energy Conv. Manag., 207, 2020, doi:10.1016/j.enconman.2020.112494.

Declaration of interests

The authors declare that they have no known competing financial interests or personal relationships that could have appeared to influence the work reported in this paper.

Acknowledgements

This research did not receive any specific grant from funding agencies in the public, commercial, or not-for-profit sectors.